



**HAL**  
open science

## Concomitant behavior of arsenic and selenium from the karst infillings materials of the fractured carbonate Dogger Aquifer (Hydrogeological Experimental Site, Poitiers, France)

R. Mhanna, A. Naveau, Maïté Bueno, M. Shmeit, F. Ismail, C. Fontaine, G. Porel, J. Bassil, L. Caner

### ► To cite this version:

R. Mhanna, A. Naveau, Maïté Bueno, M. Shmeit, F. Ismail, et al.. Concomitant behavior of arsenic and selenium from the karst infillings materials of the fractured carbonate Dogger Aquifer (Hydrogeological Experimental Site, Poitiers, France). *Chemosphere*, 2021, 275, pp.129935. 10.1016/j.chemosphere.2021.129935 . hal-03169005

**HAL Id: hal-03169005**

**<https://univ-pau.hal.science/hal-03169005v1>**

Submitted on 10 Mar 2023

**HAL** is a multi-disciplinary open access archive for the deposit and dissemination of scientific research documents, whether they are published or not. The documents may come from teaching and research institutions in France or abroad, or from public or private research centers.

L'archive ouverte pluridisciplinaire **HAL**, est destinée au dépôt et à la diffusion de documents scientifiques de niveau recherche, publiés ou non, émanant des établissements d'enseignement et de recherche français ou étrangers, des laboratoires publics ou privés.



Distributed under a Creative Commons Attribution - NonCommercial 4.0 International License

1 **Concomitant behavior of arsenic and selenium from the karst infillings**  
2 **materials of the fractured carbonated Dogger aquifer (Hydrogeological**  
3 **Experimental Site, Poitiers, France)**

4  
5 **R. Mhanna<sup>1</sup>, A. Naveau<sup>1</sup>, M. Bueno<sup>2</sup>, M. Shmeit<sup>1</sup>, F. Ismail<sup>1</sup>, C. Fontaine<sup>1</sup>, G. Porel<sup>1</sup>, J.**  
6 **Bassil<sup>3</sup>, L. Caner<sup>1</sup>**

7 <sup>1</sup> Université de Poitiers, UMR 7285 IC2MP-HydrASA, TSA 51106, 5 rue Albert Turpain, 86073  
8 Poitiers Cedex 9, France.

9 <sup>2</sup> CNRS/Univ. Pau & Pays de l'Adour/E2S UPPA, Institut des Sciences Analytiques et de Physico-  
10 Chimie pour l'Environnement et les Matériaux (IPREM), UMR 5254, 64053 Pau, France

11 <sup>3</sup> L2GE, Lebanese University, Faculty of Sciences 2, Fanar, Matn, Lebanon  
12

13 **Abstract**

14 Petrographic and mineralogical analyses combined with sequential extractions and leaching  
15 experiments as a function of pH were performed on black clayey sediments fulfilling karsts in the  
16 Hydrogeological Experimental Site (HES) of Poitiers (France) to investigate the behavior of arsenic and  
17 selenium in a fractured limestone aquifer.

18 Sequential extractions showed that arsenic is mainly associated with pyrite (about 35%) and secondary  
19 iron oxyhydroxides (around 13%), along with a substantial exchangeable fraction (about 13%). The  
20 soluble and associated to organic matter fractions are < to 2% and ~ 5% respectively. The distribution  
21 of selenium is mainly pyritic (around 39%) or associated with organic matter (about 18%). Its  
22 association to secondary iron oxyhydroxides minerals is low (around 2%) whereas its soluble fraction is  
23 around 5%.

24 SEM analyses revealed the presence of arsenic “hot spots” into euhedral pyrite crystals surrounded by a  
25 halo of iron oxyhydroxides resulting from their alteration both of which are enriched with arsenic.  
26 Selenium has a similar pyritic origin but after alteration, it is predominantly associated with organic  
27 matter.

28 Despite different distributions, the leaching experiment as a function of pH showed that the  
29 mobilization of arsenic and selenium overlapped below pH 2 and above pH 8. The main differences are  
30 observed between pH 2 and pH 8 with a plateau at 5% of released selenium, whereas the amount of  
31 mobilized arsenic continuously decreases. The pH-dependence of both elements is attributed to the  
32 partial dissolution of pyrite in acidic conditions combined with desorption processes for higher pH  
33 values.  
34  
35  
36  
37

## 39 **1 Introduction**

40

41 Arsenic (As) and selenium (Se) are trace elements normally present in scarce amounts in water bodies.  
42 However, their cumulative build-up can cause detrimental effects on human health, including several  
43 types of cancer (Chen et al., 1992; Tamoto et al., 2015). As a result, the European Union established  
44 standards at 10 µg/L in 1998 (European Union, 1998) for both elements as limits of consumption in drinking  
45 water. Both elements exist as oxyanions and their speciation is controlled by different factors, such as  
46 pH, redox conditions (Eh), water composition, and dissolved oxygen (DO) (Rosen and Liu, 2009). The  
47 inorganic species are usually more harmful than the organic ones, and the most common forms found in  
48 nature are arsenite (AsIII) and arsenate (AsV) for arsenic, and selenite (SeIV) and selenate (SeVI) for  
49 selenium (Smedley and Kinniburgh, 2002; Nakamaru and Altansuvd, 2014; Tabelin et al., 2017).

50 The mechanisms that control the mobility of these elements firstly depend on the solubility of the  
51 primary bearing-minerals, such as sulfides, arsenides, and selenides. The first steps of mobilization are  
52 related to dissolution/precipitation processes and/or associated sorption/desorption reactions (Wilkin et  
53 al., 2018). Geogenic sources of As and Se were reported in aquifers of many countries around the world  
54 (Raessler, 2018; Wilkin et al., 2018). Common secondary phases in sediments are responsible for the  
55 retention of both elements, such as carbonates, ox-hydroxides, organic matter, sulfides, and clay minerals.  
56 Thus, to correctly assess the environmental behavior of the two elements, it is important to investigate  
57 their distribution and their geochemical associations in sediments as well as their potential mobility  
58 under different environmental conditions.

59 Parallel and sequential extractions are simple and effective methods that provide insights into the  
60 bioavailability, mobility, carrier phases, and release mechanisms of trace elements into water bodies  
61 (Tessier et al., 1979). They have been extensively used to assess the various distribution of As and Se in  
62 different solid constituents (Bassil et al., 2016; Javed et al., 2014; Kim et al., 2014; Martens and Suarez,  
63 1997; Wenzel et al., 2001). Javed et al. (2014) showed that arsenic was mainly present in sulfide-  
64 bearing minerals in shale deposits and specifically sorbed on the mineral and organic phases. Likewise,  
65 Kim et al. (2014) showed that arsenic was mainly retained by sulfide minerals and their weathering  
66 products, including iron oxides, in the studied soils. On the other hand, Kulp and Pratt (2004) reported  
67 that sulfide minerals, mainly pyrite, and organic compounds were the predominant carriers for selenium  
68 in organic-rich chinks and shales. Similar results obtained by Matamoros-Veloza et al. (2011) revealed  
69 that the primary hosts for Se in various shales in the world are pyrite and organic matter, but they  
70 considered that selenium had a higher affinity for pyrite at lower concentrations.

71 In addition to chemical extraction, the analyses of the pH effect on the leachability of As and Se  
72 helps to better identify the carrier phases and their release mechanisms into the environment  
73 (Jegadeesan et al., 2008; Tabelin et al., 2014; Tamoto et al., 2015; Wang et al., 2018).

74 Selective extractions and leaching experiments of previous studies in the Dogger aquifer highlighted the  
75 diversity of the selenium distribution into the continental sedimentary clay karst infilling material  
76 inducing multiple release mechanisms (Bassil et al., 2018, 2016a). The presence of soluble selenium in  
77 different wells of the HES was nevertheless mainly attributed to the relatively important easy-  
78 mobilizable Se fraction. The mobility of this fraction seemed to be mainly ruled by its association with  
79 the organic matter present in the argillaceous samples.

80 The groundwater from the Dogger aquifer of the Hydrogeological Experimental Site (HES) of Poitiers  
81 exhibits soluble selenium concentrations ranging between 10 and 40  $\mu\text{g/L}$  in different wells whereas no  
82 detectable presence of arsenic was quantified (Bassil et al., 2016a, 2018). These behaviors contrast with  
83 the chemical composition of the associated sedimentary materials, which contain about fourfold higher  
84 arsenic than selenium (Bassil et al., 2016a, 2018). Even though the karsts partially filled by clayey  
85 sediment are discontinuous in the mid-Jurassic limestone, they represent an important rock-source of As  
86 and Se at the regional scale for Dogger aquifer.

87 Many studies examined the leaching behaviour of arsenic and selenium concomitantly (Su and Wang,  
88 2011; Tabelin et al., 2014; Wilkin et al., 2018b; Yang and He, 2016). However, studies with systematic  
89 comparisons between the geochemical behavior of As and Se are limited. In the present study, we  
90 focused on comparing the distribution and behavior of the two elements in dark argillaceous sediments  
91 found in karstic cavities of the mid-Jurassic aquifer. The primary objectives are: (1) performing  
92 petrographic investigations using optical microscopy, scanning electron microscope coupled with  
93 energy dispersive X-ray (SEM-EDX), and X-ray diffraction; (2) evaluating the distribution of As and  
94 Se using parallel and sequential extractions; (3) examining the effect of pH on their release; (4)  
95 correlating the occurrences of As and Se as well as the coexisting ions and geochemical parameters.  
96 Finally, all data have been statistically analyzed based on the null hypothesis i.e. by assuming that the  
97 behaviors of arsenic and selenium are different.

98

## 99 **2 Materials and Methods**

### 100 **2.1 Site description, sampling, and preparation**

101 This study was carried out on the Dogger aquifer of the Hydrogeological Experimental Site (HES) of  
102 Poitiers. The HES consists of a research platform of the University of Poitiers and belongs to the  
103 SOERE H+ Network (<http://hplus.ore.fr/>) dedicated to long-term monitoring and understanding  
104 groundwater flow and solute transfer in heterogeneous carbonate aquifer (Audouin et al., 2008; Le Coz  
105 et al., 2017, Mari et al., 2020). The Dogger aquifer corresponds to carbonates of Middle Jurassic age of  
106 about 100 m thick (~20 to ~130 m from ground level) with the presence of pervasive karstic caves and  
107 conduits (Mari et al., 2020) partially infilled by clayey sediments of various composition and color. The  
108 studied samples were collected in 2012 through non-destructive drilling at a depth between 66 m and 71  
109 m in a borehole called C5 that crosses the Dogger aquifer of the HES. The collected samples are clayey

110 sediments enriched in organic matter, pyrite, and selenium that fulfill a part of the karst cavities  
111 developed within the Bajocian limestone host rocks, as described by Bassil et al. (2016b).

112 Extensive characterizations dated the selected samples from the Upper Cretaceous and showed the  
113 external and continental origin of the infilling materials and their transformation after deposition under  
114 reducing conditions (Bassil et al., 2016b).

## 116 **2.2 Instrumentation and Analysis**

### 117 **2.2.1 Characterization of the sedimentary sample**

118 The total elemental composition of the sample C5-BjF was determined by ICP-MS after LiBO<sub>2</sub> fusion  
119 and acid dissolution in an accredited laboratory (CRPG-CNRS, Nancy, France - <http://www.crbg.cnrs-nancy.fr/SARM/index.html>), by CHNS analysis (Flash 2000 Thermo, IC2MP, France) for the organic C  
120 and total S, and by ICP-MS for total As and total Se (Agilent 7500ce, IPREM, France).

122 Powdered samples (infra 50 µm fraction) were analyzed by X-ray diffraction (XRD) using a Phillips  
123 Panalytical X'Pert Pro apparatus in the same experimental conditions as described by Bassil et al.  
124 (2016b).

125 The phase identifications were made with the X'pert HighScore software, while the semi-  
126 quantifications were obtained by applying the RIR method (Chung, 1975; Hillier, 2000) to major peak  
127 areas. The RIR values used for the identification are available in JCPDS Pdf2 mineralogical database.  
128 Based on experimental peaks correction using corundum (□-Al<sub>2</sub>O<sub>3</sub>) as an external standard, this  
129 method is simple and efficient when clay minerals do not have specific chemical compositions and  
130 show great variabilities of peak intensities due to structural disorder (Xiang et al., 2018), which is the  
131 case for the kaolinite-rich studied samples.

132 Diffractograms presented in Figure 1 were normalized to the peak intensity of kaolinite at 7.19 Å.

133 Thin sections (26x46mm; 30 µm thickness) were prepared from undisturbed samples after impregnation  
134 at room temperature and under atmospheric pressure with a two-component epoxy resin (Araldite 2020)  
135 diluted with 20% acetone. The thin sections were observed using an optical polarized light microscope  
136 (Nikon Eclipse E600 POL) and then using a scanning electron microscope JEOL 5600-LV [Low  
137 Vacuum] (IC2MP, UP, Poitiers) equipped with a secondary electron detector Everhart – Thornley and a  
138 backscattered electron detector Centaurus (KE Development ic, Cambridge) with a Bruker energy  
139 dispersive X-ray spectrometer for scanning electron microanalyses (SEMA). Additional pictures were  
140 obtained using a scanning electron microscope Jeol JSM-7900F. The pictures were obtained at working  
141 distances of 10 mm and an accelerating voltage of 20 kV. Data processing was provided by the  
142 chemical analysis software QUANTAX.

### 146 2.2.2 Chemical extractions

147 Protocol choices were based on a compromise between different classical extraction schemes developed  
148 for arsenic and selenium (Bassil et al., 2016a; Javed et al., 2013; Kim et al., 2016, 2014; Martens and  
149 Suarez, 1997; Wenzel et al., 2001; Zhang and Jr, 2003). A series of multiple parallel extractions (**Table**  
150 **1**) were therefore tested to develop a six-step extraction protocol that targets both arsenic and selenium  
151 phases. The protocol was thus applied in a sequential scheme with two different contact times, described in  
152 **Table 2**. In addition, the release of potentially interesting elements (Fe, Mn, Ca, Mg, Al, Si, TOC) was  
153 monitored to have an insight into the possible solid phase carriers.

154 The sediment (C5-BjF) used in this study was preserved since 2012 at low temperature (-18°C) under an  
155 argon atmosphere. For this protocol, the sample was freeze-dried, ground into a powder with agate  
156 mortar, and then sieved at 200 µm. Solid suspensions containing 600 mg of powdered solid and 20 ml  
157 of the extraction solution were then prepared directly in centrifuge tubes to minimize the possible loss  
158 between the different steps. Tubes were closed during the extraction period and agitated at a speed of 350  
159 rpm. Suspensions were then centrifuged for 10 min at a speed of 14,000 rpm using Thermo Scientific  
160 Heraeus biofuge stratos and then filtrated through a 0.45 µm Sartorius nylon membrane. The  
161 equilibrium pH of the supernatant was measured by a pH meter Metrohm 827 immediately after  
162 separation. Recovered supernatants were stored at 4°C before further analysis. The next extraction  
163 solution was added to the remaining residue of each step. Solid residues obtained at the end of the sequential  
164 extractions scheme were oven-dried for 1 week at 105°C, ground with agate mortar, and stored for  
165 mineralogical analyses. The residual fraction was calculated by subtracting the total released element  
166 during extraction, from the total concentration. All the chemical reagents used were of analytical grade.  
167 The used ultrapure water was obtained from the Milli-Q system (18.2 MΩ.cm<sup>-1</sup>, Elix, Millipore).

168

### 169 2.2.3 Chemical Analyses

170 Quantifications of As and Se in the extracted solutions were performed by ICP-MS (Agilent 7500ce,  
171 IPREM, France) with operating conditions as described by Bassil et al. (2016a) except the use of H<sub>2</sub>-He  
172 mixture (3.5-1.5 mL min<sup>-1</sup>) for the octupole collision/reaction cell. The AAS (Varian AA24FS, IC2MP,  
173 France) was used for the quantification of major elements and ICP-OES (Agilent Technologies 5110,  
174 IC2MP, France) for Si and Al. Speciation of arsenic and selenium was performed by HPLC coupled to  
175 the same ICP-MS used for total As and Se measurements. The chromatographic system consisted of an  
176 Agilent 1100 series HPLC pump, equipped with an autosampler and variable volume sample loop. The  
177 HPLC-ICPMS interface was made up of a polyetheretherketone (PEEK) tube. Chromatographic  
178 separation was carried out on anion exchange stationary phase (Agilent G3154 column 15 cm × 4.6 mm  
179 i.d) with ammonium nitrate mobile phase (20 mmol L<sup>-1</sup>, 2,5% methanol and pH 8.5 adjusted with  
180 ammonia) delivered at 1 mL min<sup>-1</sup> flow rate. Selected chromatography allowed the separation of  
181 arsenite, arsenate, selenite, and selenate species.

#### 182 **2.2.4 Batch leaching experiments**

183 Batch leaching experiments were performed at ambient temperature in borosilicate flasks in which  
184 suspensions were prepared by mixing the sample C5-BjF with ultrapure water during a contact time of  
185 1 week and under agitation with a reverse system at 30 rpm. The pH was adjusted at the beginning of  
186 the experiment by the addition of 1 M NaOH or HCl and the equilibrium pH of the supernatant was  
187 measured directly after separation.

188 The preparation of the sedimentary sample, the SL ratio, the separation method, the storage conditions,  
189 and the quantifications of the leachates were carried out as described in part 2.2.2.

190

#### 191 **2.2.5 Statistical studies**

192 The statistical analyses were performed using R studio. Correlation coefficients were calculated using  
193 Pearson's method with a confidence interval of 5%. Correlation tables related were performed with 6  
194 reagents and 6 parameters for extraction experiments and 12 acid/base conditions and 6 or 9 parameters for  
195 leaching experiments.

### 196 **3 Results and discussion**

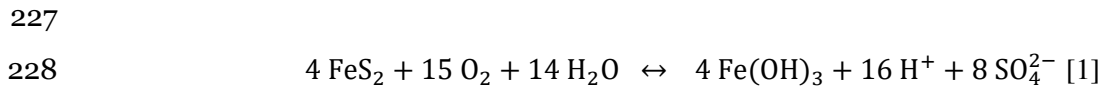
#### 197 **3.1 Chemical, mineralogical and petrographical characterizations**

198 The karst infilling material C5-BjF is composed of a clayey matrix (mainly kaolinite and smectite to a  
199 lesser extent) with traces of detrital materials such as quartz, feldspars, and titanium oxides as described  
200 by Bassil et al. (2018) for a similar sedimentary sample (C5-BjC). Calcite and pyrite contents are  
201 present at relatively low amounts and the amount of organic matter (5.7%) probably explains the dark  
202 color of the sample (Table 3 + Figure 2).

203 The studied materials are composed of a brownish clayey matrix (FM for Fine Materials) containing  
204 many clasts (CM for Coarse Materials), heterogeneous in size and nature, and partially weathered by  
205 the organic matter in contact (Figure 2A). The matrix is also crossed by a dense network of subparallel  
206 cracks and coated by a black film attributed to organic matter and infilled by clayey material (Figure 2B  
207 and 2C). The infillings are polyphased (Figure 2C) and composed of a mixture of cream-white areas  
208 attributed to carbonates and orange/brown areas attributed to iron-oxy-hydroxides and are indicative  
209 periods of humectation/desiccation suffered by the deposit.

210 Scanning electronic microscopy mainly focused on the numerous pyrite crystals (bright areas due to the  
211 presence of iron) within the clayey matrix (Figure 3). Three main habitus were identified, as observed  
212 by Bassil et al. (2016b), suggesting different mechanisms of formation. Euhedral pyrite (EP), generally  
213 formed by direct nucleation and growth in a supersaturated solution, is present locally as micrometric  
214 crystals. Large framboidal pyrite (FP) is the main morphology encountered. It results from the  
215 transformation of greigite  $Fe_3S_4$  as a precursor without consensus regarding the involvement of bacterial  
216 activity in their formation (Sawlowicz et al., 2005; Wilkin et al., 1996). An intermediate pyrite  
217 morphology (IP) is also observed formed due to the progressive cementation of porosity during

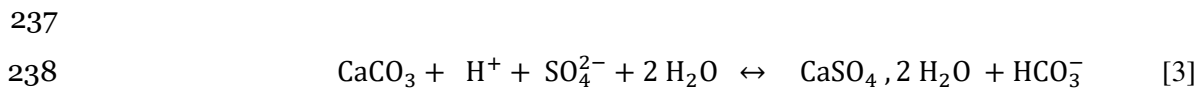
218 diagenesis as shown by the overgrowth of microcrystals recrystallized into unfilled framboid and/or  
219 euhedral pyrite crystals (Sawlowicz et al., 2005). The spots that appear in bright spots in Figure 3A are  
220 associated with the presence of Fe and S (Figure 3B and 3D), which confirms the pyritic areas. In other  
221 domains, the diffuse distribution of S is partially correlated with the diffuse distribution of calcium  
222 (Figure 3F), indicative of the presence of gypsum (not detected on XRD patterns probably due to low  
223 bulk concentration). The Ca-rich areas correspond to the calcite location. Likewise, the diffuse halos of  
224 Fe around the pyritic crystals but uncorrelated with sulfur can be attributed to iron oxyhydroxides.  
225 These observations could be explained by the oxidation of pyrite followed by the reprecipitation of  
226 secondary iron oxyhydroxides according to Equation 1 (Ritsema et al., 1992):



229  
230 The resulting local acidic medium (vicinity of oxidized pyrites) was neutralized by a reaction between the  
231 released protons and the neighboring carbonates— predominantly calcite from the limestone host in the  
232 studied case - according to Equation 2 (Ritsema et al., 1992):



235  
236 The released calcium reacts with sulfate to form gypsum according to Equation 3 (Ritsema et al., 1992):



239  
240 The diffuse distribution of Si and Al (Figure 3C and 3E), which is reverse to that of Fe and S is related  
241 to the abundance of clay minerals in the sediment.

242 Natural pyrite lattices are important hosts of minor and trace elements such as As, Se, Ni, Mo, Co, Cu,  
243 Zn, and Pb. The SEM observations and chemical analyses highlighted arsenic “hot spots” in  
244 pyrites (Figure S1). These “hot spots” were only observed in the euhedral pyrites whereas, no  
245 significant increase of arsenic content was detected in the framboidal pyrites, clay minerals, or  
246 carbonates. By contrast, pyrite associated Se was probably not detected owing to the lower bulk  
247 concentration of selenium (6.3 mg/kg) compared to that of arsenic (22.4 mg/kg), rendering the selenium  
248 content below the detection limit of the EDX detector.

249 As the euhedral pyritic crystals enriched in arsenic have large diameters, a formation by precipitation in  
250 the porosity of the sediment after deposition is assumed in accordance with Bassil et al. (2016b).

251

252

253

254 **3.2 Single parallel extractions (Table 4)**

255 **3.2.1. Easily mobilized fractions of arsenic and selenium**

256 Extractions with purified water, a sulfate solution, or a phosphate buffer are expected to only mobilize  
257 As or Se oxyanions that are water-soluble or weakly sorbed (outer-sphere complexation for ammonium  
258 sulfate and inner-sphere-complexation for phosphate buffer) onto the matrix surface (Javed et al., 2013;  
259 Wenzel et al., 2001).

260 The corresponding fractions (soluble and exchangeable) are expected to represent the immediately  
261 available As and Se fractions in the HES groundwater. In the present study, about 5% of selenium is  
262 soluble (and no significant exchangeable fraction) whereas the easily mobilized As fraction is mainly  
263 exchangeable (around 20% against less than 2% for the soluble one).

264 The speciation of selenium in the soluble fraction mainly consists of SeVI which is consistent with the  
265 species regularly quantified in several wells from the HES. The speciation of arsenic in the soluble  
266 fraction is a mixture between AsIII (around 60%) and “non-identified” As, while the arsenic in the  
267 specifically-sorbed fraction is exclusively AsV. In the collected groundwater samples from the HES,  
268 AsV is predominant even if high uncertainties are related to the quantifications by HPLC-ICP-MS of  
269 the soluble As fraction due to the low measured concentrations (less than 1 µg/L).

270 No significant mobilization of aluminum and iron was observed in these fractions supporting anionic  
271 exchange mechanisms. Nevertheless, significant amounts of calcium (and magnesium to a lesser extent)  
272 were quantified in the soluble fraction (nearly 2%), the non-specifically sorbed one (around 70%), and  
273 the specifically sorbed one (around 8%).

274 The behaviors of arsenic and selenium do not seem to be linked to the dissolution of carbonates,  
275 although it is not excluded that calcite is an effective scavenger of trace elements including arsenic and  
276 selenium (Costagliola et al., 2013; Renard et al., 2015; Rios-Valenciana et al., 2020).

277  
278 **3.2.2. Fraction of arsenic and selenium associated with carbonates**

279 Selenium released concomitantly with the dissolution of carbonates (calcite, and dolomite to a lesser  
280 extent) is comparable to the soluble Se fraction observed in the previous paragraph and suggesting that  
281 no detectable selenium is trapped into the carbonated matrix. This observation is consistent with the  
282 results of Bassil et al.(2016a) performed with a similar sample (Table 3) and supports that the origin of  
283 selenium in the Dogger aquifer is related to the clayey karst infilling materials and not to the limestone  
284 host.

285 Arsenic fraction associated with carbonates (about 15%) seems to be included in the exchangeable As  
286 fraction (about 20%). This observation suggests that no detectable arsenic is present in the carbonates  
287 and also tends to show that acetate buffer through its carboxylate group favors the release of  
288 specifically sorbed arsenic, less efficiently than phosphate ions or as efficiently with a later  
289 reprecipitation or re-complexation of arsenic.

### 290 **3.2.3. Co-precipitated fraction of arsenic (and selenium) with amorphous Fe oxyhydroxides**

291 Significant amounts of iron (II and III) were quantified in the studied sample, but only pyrite was  
292 detected by XRD measurements (Table 3). These observations could be explained by the presence of  
293 amorphous or poorly crystallized FeIII oxyhydroxides identified by SEM/EDX but hardly detected by  
294 XRD or by a low occurrence of crystallized Fe-containing minerals.

295 In parallel, petrographic investigations show the presence of pyritic crystals altered into gypsum and  
296 iron-bearing minerals such as poorly crystallized oxides or oxyhydroxides (Figure 3). After weathering,  
297 arsenic initially associated with pyrite could have been coprecipitated with iron minerals or possibly  
298 reprecipitated as scorodite in the immediate vicinity (Kim et al., 2015).

299 Ammonium oxalate buffer was used to enhance the dissolution of poorly crystallized iron-bearing  
300 minerals (Paniás et al., 1996) according to the following sequence: (1) adsorption of the carboxylate  
301 group onto the surface, (2) non-reductive dissolution through direct desorption, and then (3) reductive  
302 dissolution of iron. During the reduction phase, visible light mediates electron transfer on the surface of  
303 ferric-oxalate complexes providing a supplementary pathway for the dissolution of oxides. Dark  
304 conditions were thus preferred to limit an over-estimation of released arsenic.

305 Arsenic release associated with poorly crystallized iron oxyhydroxides is significantly higher (nearly  
306 35%) than the amounts mobilized with the previous single extractants, supporting the assumption that  
307 after pyrites weathering, the arsenic initially present in their structure could have coprecipitated with  
308 secondary iron minerals or reprecipitated as scorodite ( $\text{FeAsO}_4 \cdot 2\text{H}_2\text{O}$ ) in the immediate vicinity (Kim  
309 et al., 2015). Iron release corresponds only to around 5%, confirming the relatively high proportion of  
310 arsenic associated with secondary iron oxides and oxyhydroxides.

311 The speciation of released arsenic with the oxalate buffer is mainly AsV as observed with the  
312 exchangeable fraction and consistently with the speciation generally observed for scorodite or  
313 coprecipitated iron phases (Kim et al., 2015).

314 Even if all the calcium released has been reprecipitated as calcium oxalate, the presence of soluble  
315 magnesium tends to show that carbonates (calcite and dolomite) were also dissolved concomitantly to  
316 amorphous iron minerals.

317 Despite the low pH (Table 1), no significant amount of soluble aluminum was quantified in the  
318 extraction solution suggesting the absence of amorphous Al-bearing minerals.

319 Selenium release slightly increases (around 7.5%) compared to the soluble Se fraction (around 5%) and  
320 could be attributed to a specifically sorbed Se fraction onto iron-bearing minerals (Börsig et al., 2017;  
321 Fernández-Martínez and Charlet, 2009).

322

### 323 **3.2.4. Reducible fraction of arsenic (and selenium)**

324 Reducing agents of different strengths (sodium dithionite (RedA), ascorbic acid (RedB), and  
325 ammonium oxalate (RedC)) were tested to both favor the dissolution of iron-bearing minerals and  
326 enhance the solubility of arsenic through reduction of AsV into AsIII. Combinations with a strong

327 chelating agent (EDTA) were also performed to limit the interactions between arsenic oxyanions and  
328 the ferrous soluble species or the newly formed iron oxide phases (Kim et al., 2015). None of the  
329 extractants (EDTA alone, reducing agent alone, or a mix) was more efficient to mobilize arsenic from  
330 the studied sample than the oxalate buffer despite a higher mobilization of iron in the presence of  
331 EDTA (6.1% against 4.6% with the oxalate buffer). Even if relatively well-crystallized iron oxides  
332 could be targeted in the present fraction, reprecipitation and recomplexation of arsenic onto the surfaces  
333 is expected and EDTA seems to be the limiting factor.

334 No mobilization of selenium was expected with reducing agents, but sodium dithionite generates an  
335 important release of selenium (nearly 20%). This observation is explained by the inherent instability of  
336 dithionite that can produce powerful oxidizing radicals for selenium compounds (Geoffroy and  
337 Demopoulos, 2009) or the formation of colloidal elemental selenium that could pass through filtration  
338 membranes. The important release of selenium with ascorbic acid (about 18%) tends to favor this  
339 second assumption.

340 No significant amount of soluble aluminum was quantified whereas all the initial calcium was  
341 mobilized in the presence of EDTA. Reprecipitation of calcium oxalate was also observed by XRD.

### 342 **3.2.5. Oxidizable fraction of selenium (and arsenic)**

343 Sodium hypochlorite (NaOCl) is an efficient extractant of organic matter however, no significant  
344 fraction of arsenic was extracted using this reagent (comparable release as the exchangeable fraction).  
345 The amount of Se extracted by NaOCl, on the other hand, was significant (about 10% estimated by  
346 difference).

347 Surprisingly, an important amount of arsenic (around 40%) was mobilized with the oxidizing agent  
348 sodium sulfite. This reagent associated with light and iron can generate the photooxidation of AsIII into  
349 AsV but this reaction is highly sensitive to the initial amount of sulfite and the pH conditions (Xu et al.,  
350 2016). In other conditions (Zakharova et al., 2015), sodium sulfite can also be used as a photo-reductive  
351 reagent.

352 The present reagent targeted the elemental selenium initially present in the sediment and generated  
353 unexpected reactions with the arsenic initially present in the sediment but further investigations onto the  
354 speciation of the released arsenic should be necessary to better understand the processes involved in the  
355 present case.

356

### 357 **3.2.6. Alkaline-soluble fraction of arsenic and selenium**

358 The studied karst infillings contain relatively high amounts of organic matter (**Table 3**), degradation  
359 products of vascular plants that have been transported from the surface into karst cavities (Bassil et al.,  
360 2016a). Associations between the humic-like organic matter and arsenic and selenium were targeted  
361 using different concentrations of sodium hydroxide (NaOH 0.1, 0.5, and 1 M).

362 A significant alkaline-soluble fraction for both arsenic and selenium is observed but the concentration  
363 of sodium hydroxide has no influence on the mobilization of arsenic (around 40%) and selenium

364 (around 25%). Concomitantly, the lowest basic conditions clearly enhance the mobilization of  
365 aluminum (about 8%) and iron (about 10%) whereas the amount of organic C released (around 10%)  
366 tends to increase with increasing basic conditions. Similar results were observed with different  
367 proportions (85% of Se released and 21% of organic C and 2% Fe released) by Bassil et al. (2016a)  
368 who have attributed the partial mobilization of iron in alkaline conditions to the presence of complexed  
369 species.

370 No significant release of Si was observed suggesting the absence of dissolution of the clay minerals as  
371 confirmed by the corresponding X-ray diffractograms (figure 1).

372 The As fraction associated with the organic matter is thus estimated at around 5% with a speciation  
373 corresponding to a mix between AsIII (around 23%) and AsV (around 77%), whereas the Se alkaline-  
374 soluble fraction tends to reach about 10%.

### 375 376 **3.2.7. Fraction of arsenic and selenium associated with pyrite**

377 As expected by the mineralogical and petrographic investigations, a significant As pyritic fraction was  
378 extracted using hot nitric acid. In addition, a significant Se fraction was also observed at this step.

379 The pyritic fraction can be thus estimated by subtraction at around 15% and 20%, for arsenic and  
380 selenium, respectively. Under hot nitric treatment, the mobilization of the studied elements is parallel to  
381 the mobilization of almost all the iron - and the calcium - content of the sedimentary sample,  
382 confirming the low selectivity of this reagent (Kulp and Pratt, 2004), but also involving the mobilization  
383 of arsenic “trapped” with all the iron-bearing minerals, both primary (sulfides) and secondary (oxides  
384 and oxy-hydroxides).

### 385 386 **3.2.8. Synthesis of single parallel extractions**

387 In addition to the significant soluble Se fraction (about 5%), consistent with the presence of selenium  
388 species quantified in different wells drilled into the Dogger aquifer of the HES, this element seems to be  
389 associated with pyrite and to a lesser extent to their alteration products but also to the organic matter.  
390 Neither significant association with the carbonates nor the presence of elemental selenium was  
391 highlighted by the present series of single parallel extractions.

392 Concerning arsenic, a very low soluble fraction was observed compared to its relatively important  
393 exchangeable fraction (about 20%). As for selenium and consistently with the microscopic  
394 investigations, the distribution of arsenic seems to be mainly limited to the pyritic crystals and the  
395 secondary iron-bearing minerals present in the sedimentary clayey matrix.

396 Statistical analyses (Figures S4 and S5) support the present observations by highlighting the high  
397 correlation coefficients between the released amounts of arsenic and iron ( $r = 0.78$ ), selenium and iron  
398 ( $r = 0.89$ ), and arsenic and selenium ( $r = 0.87$ ). In parallel, no significant positive correlation was shown  
399 between the three previous elements and calcium, aluminum, or pH conditions.

400

401

### 402 **3.3 Sequential chemical extraction**

403 To refine the major points brought to light by the series of parallel extractions experiments, a simplified  
404 sequential extraction scheme (Table 2) was defined using both the results of paragraph 3.2. and the  
405 characterization of the sedimentary matrix (paragraph 3.1.). Two contact times– except for NaOH –  
406 were also tested to better understand the effect of contact time on the mechanisms involved in the  
407 release of the two elements.

408

#### 409 **3.3.1. Behaviour of arsenic**

410 In accordance with the parallel extractions, the easily mobilized fraction of arsenic is mainly  
411 exchangeable (about 13%) with a low soluble fraction (less than 2%) (Figure 4A). A longer contact  
412 time has no impact on the soluble fraction but significantly increases the exchangeable one (from 13.3%  
413 to 22.2%) (Figure 4B). This point could be of high concern *in-situ* leading to an important arsenic  
414 mobilization due to slight changes in the ionic composition of the groundwater induced by pumping or  
415 climatic changes (Smedley and Kinniburgh, 2002).

416 A low but significant As fraction associated with the carbonates (about 8.5%) was identified by the  
417 sequential scheme contrary to the parallel one and tends to decrease with a longer contact time (Figure  
418 4). It is assumed that part of this fraction was extracted in the previous steps, the dissolution of  
419 carbonates being favored by longer contact times. But, in the present case, the amounts of mobilized  
420 calcium totally invalidate this assumption and tend to support that the arsenic associated with calcite  
421 may be released by other mechanisms, such as the desorption of weakly-sorbed fraction (Rios-  
422 Valenciana et al., 2020). It is to note that all the calcium has been extracted at this step, as confirmed by  
423 the chemical and mineralogical analyses (Figures S1 and S2).

424 The As fraction associated with alteration products of the pyritic materials, described through SEM-  
425 EDX pictures as diffuse and poorly crystallized iron oxides corresponds to about 13% of the total  
426 arsenic initially present in the matrix, consistently with the estimation performed with the parallel  
427 extractions. The amount of mobilized iron is refined to 7.4% and slightly increases for a longer contact  
428 time to 8.3%. The concomitant decrease of the As release is attributed, as for the fraction associated  
429 with the carbonates, to a partial extraction of this fourth fraction during the longer contact time with  
430 phosphate buffer whose pH and complexing properties cannot prevent iron reprecipitation.

431 The As fraction associated with organic matter is relatively low (less than 5%) in accordance with the  
432 parallel extractions, whereas the pyritic fraction is the most important (about 35%) as expected by the  
433 elemental spatial distribution (Figure S1). This amount was highly underestimated by parallel  
434 extractions whereas all the iron was mobilized. This amount is not dependent on the contact time and  
435 tends to show that about 80% of the iron present in the matrix was initially pyritic.

436 About 25% of arsenic was finally refractory to the present sequential extraction scheme, assumingly as

437 well-crystallized As oxides or sulfides or coprecipitated with the 7.5% of refractory iron (Javed et al.,  
438 2013).

439

### 440 **3.3.2. Behaviour of selenium**

441 In accordance with the parallel extractions and the presence of selenium in the HES groundwater, the  
442 easily mobilized fraction of selenium is mainly soluble (about 5%) with a low exchangeable fraction  
443 (less than 1%). A longer contact time seems to slightly increase the soluble fraction at the expense of  
444 the exchangeable one. This point could explain the progressive increase of the selenium concentrations  
445 measured in the HES wells poorly connected to the other wells and thus containing stagnant waters (not  
446 published).

447 No significant Se fraction associated with the carbonates was quantified as estimated by parallel  
448 extractions experiments supporting that selenium was not originated from the limestone host of the  
449 Dogger aquifer. The fraction associated with secondary iron-bearing minerals and probably specifically  
450 sorbed onto their surface is low (about 2%), whereas the Se fraction associated with organic matter is  
451 relatively important (nearly 18%). The contact time has no significant influence on the amounts  
452 released.

453 As observed for arsenic, the Se pyritic fraction was highly underestimated by parallel extractions and  
454 reached 39% of the initial selenium in the matrix. This amount suggests the presence of pyrite-  
455 associated selenium that was not observed by SEM-EDX.

456 The important refractory Se fraction (around 37%) is attributed to the absence of adapted reagents  
457 (mainly oxidizing reagents targeting elemental and organic selenium) in the sequential scheme.

458

### 459 **3.3.3. Synthesis of sequential extractions scheme**

460 The combination of petrographic and mineralogical investigations with the sequential extractions'  
461 experiments suggest that pyritic minerals are the main initial hosts of arsenic and selenium of the clayey  
462 karst infillings present in the Dogger aquifer. The alteration of these primary minerals had assumingly  
463 favored the partial mobilization of selenium and arsenic followed by reprecipitation and sorption  
464 processes with other constituents of the matrix or with secondary minerals. At this step, the pathways of  
465 selenium and arsenic tend to diverge: arsenic is mainly associated with secondary iron oxides, as  
466 already mentioned by Javed et al. (2013) in part with calcite and barely with the organic matter,  
467 whereas selenium is mainly associated with the continental organic matter as described by Gustafsson  
468 and Johnsson (1994) and Li et al. (2017), barely with the secondary iron oxides and not significantly  
469 with the limestone host.

470 Strong significant positive correlations (Figure S2) are additionally observed (and enhanced) between  
471 the released amounts of arsenic and iron ( $r = 0.94$ ) and between those of selenium and iron ( $r = 0.90$ ).  
472 Sequential extractions and longer contact times tend to decrease the correlation between arsenic and  
473 selenium ( $r = 0.75$ ) compared to single parallel experiments ( $r = 0.87$ ), supporting their divergence.

474 Concomitantly, the behaviour of aluminum seems to follow the release of selenium, iron, and arsenic.  
475 This correlation tends to be reinforced with longer contact times suggesting that more complex release  
476 mechanisms could be involved.

477 In parallel, negative correlations are observed between the released amounts of arsenic and the pH  
478 conditions ( $r = - 0.80$ ), but not for selenium ( $r = - 0.35$ ). Leaching studies as a function of pH were  
479 performed for a better understanding of the mechanisms induced in the behavior of these elements.  
480

### 481 **3.4 Leaching studies as a function of pH**

482 As previously observed by (Bassil et al., 2018; Tabelin et al., 2012), arsenic and selenium release  
483 behaviors are strongly dependent on acid-base conditions (Figure 5). In very acidic conditions (below pH  
484 2), the As (Figure 5A) and Se (Figure 5B) releases sharply increase with the pH decrease. This concomitant  
485 and consistent release behavior is attributed to the partial dissolution of pyrite, previously identified as the  
486 main host for As using the chemical extractions and SEM-EDX.

487 In basic conditions (above pH 8), the As and Se release sharply increase with the pH to reach a  
488 maximum at around pH 12 (Figure 6). These releases are again concomitant for both elements. The  
489 release fronts of Fe and Al are similar but occur at slightly higher pH (about one pH unit) than for As  
490 and Se. The release front of TOC also occurs in more alkaline conditions (about one additional pH  
491 unit).

492 As highlighted by the statistical results, Fe and Al behaviors tend to be closely correlated in basic pH  
493 conditions, as they would be complexed to the same species, probably with the humic-like organic matter,  
494 as already described for soils (Jansen et al., 2011; Wagai et al., 2013). Even if significant correlations are  
495 observed with TOC, the mobilization of the sedimentary organic matter seems to be indirectly associated  
496 with the release of other elements.

497 These observations converge to the ideas that (1) the alkaline-soluble fractions are only ruled by desorption  
498 processes and not by dissolution, contrary to the mobilizations observed in acidic pH conditions, and (2) the  
499 observed desorption processes are associated with the change in the surface charge.

500 If the behaviors of arsenic and selenium are strictly concomitant below pH 2 and above pH 8, they strongly  
501 diverge between pH 2 and pH 8. The soluble selenium is thus nearly constant at around 5% in this pH  
502 range when the mobilized arsenic decreases from about 10% at pH 2 to less than 1% at circumneutral pH.

503 It is interesting to observe that the amounts of arsenic and selenium released after 1 week of contact time in  
504 osmosed water are consistent with the amounts extracted after 2h of contact time. The soluble fraction thus  
505 consists of an easily released fraction of the studied elements. In the same way, the released amounts of  
506 arsenic (around 25%) and selenium (around 35%) in the basic plateau correspond to the ‘alkaline-soluble’  
507 fractions previously quantified for a contact time of 24 h and support rapid mechanisms.

508 In parallel, all the quantities of selenium released by selective chemical extractions are consistent with the  
509 leaching experiments and thus show that selenium mobilization is mainly governed by the acid-base

510 conditions of the medium in contact. On the contrary, the presence of complexing agents such as the ones  
511 used in the extractions experiments (phosphate, acetate, and oxalate anions), tends to favor and control the  
512 mobilization of arsenic species in the system by preventing them from reprecipitation or resorption onto  
513 surfaces.

514 Finally, as assumed by the previous experiments and statistical studies, Ca and Mg behaviors are highly  
515 related but not directly correlated to the behaviors of arsenic and selenium.

516

### 517 **3.5 Conclusion**

518 The Upper Cretaceous clayey materials that fill partly the karst cavities formed into the Bajocian  
519 limestone of the Dogger aquifer are important geogenic sources of arsenic and selenium traces found in  
520 regional groundwaters. Correlating the origin, the distribution, and the release mechanisms of these two  
521 micropollutants was expected to better understand their behaviour into a fractured carbonated aquifer.

522 The combination of petrographic investigations with chemical extractions, leaching experiments, and  
523 statistical analysis highlighted the pyritic origin of both elements. Arsenic “hot spots” were observed  
524 within euhedral pyritic crystals and into the surrounding halo of secondary iron-bearing minerals  
525 resulting from their oxidative alteration. Even though selenium-associated pyrite was not directly  
526 observed by SEM-EDX images, the chemical extractions showed the existence of an important  
527 selenium pyritic fraction. Nevertheless, the affinity of selenium for secondary iron-bearing minerals is  
528 lower than that of arsenic, and alteration of pyritic minerals has favored associations of selenium  
529 species with the humic-like sedimentary organic matter.

530 These divergences of associations have no impact on the mobilization of both elements in very acidic  
531 conditions, controlled by the partial dissolution of pyritic materials and in alkaline conditions (above pH  
532 8), ruled by desorption processes and especially by the reactivity of the involved surfaces. The main  
533 divergences in both elements’ behaviors are observed between pH 2 and pH 8, leading to a soluble  
534 fraction of about 5% for selenium and a very low soluble fraction for arsenic (lower than 2%) in the pH  
535 range [6.9; 7.9] measured in the groundwater of the Dogger aquifer.

536 The main components of the limestone aquifer (calcite and dolomite to a lesser extent) are not directly  
537 associated with the mobilization of the studied elements but, in such context, Ca-Mg-CO<sub>2</sub>-H<sub>2</sub>O  
538 equilibrium highly constrains the pH conditions of the groundwater close to neutrality. The leaching  
539 experiments also contradicted their apparent correlation with the mobilization of iron, aluminum, and  
540 TOC highlighted by previous studies and the present statistical analyses and extractions protocols.

541 Except in very acidic conditions, the behavior of selenium thus seems to be only ruled by surface  
542 complexation equilibria and therefore by the pH conditions of the medium in contact. Although the pH  
543 of the groundwater is buffered by the carbonated aquifer, local acidic conditions may occur at the  
544 vicinity of pyrites due to their oxidation. This process can be enhanced by water pumping from wells of  
545 the aquifer, which induces more oxidizing conditions.

546 The mobilization of arsenic is more complex: although the soluble fraction in percentage is very low in  
547 the pH range of the HES groundwater, the amounts of arsenic released are in the same order of  
548 magnitude as those of selenium. In parallel, even if arsenic mobilization is also highly pH-dependent  
549 and mainly ruled by sorption processes, the impact of complexing agents such as phosphate or small  
550 organic acids (acetate, oxalate) that can be naturally present in the groundwater is important (and  
551 roughly corresponds to about 20%). According to the present results, arsenic should be detected in the  
552 water sampling campaigns in the Dogger aquifer whereas it is not the case. Further investigations will  
553 thus be necessary to bring to light the impact of natural chelating agents on the stability of the surface  
554 complexes formed with arsenic and selenium species in the pH range imposed by the carbonates of the  
555 aquifer.

556

### 557 **3.6 Acknowledgments**

558 We acknowledge the financial support from the European Union, the ‘Région Nouvelle Aquitaine’ and  
559 the ‘Agence de l’Eau Loire-Bretagne’. We also acknowledge C. Boissard and J. Rousseau for their  
560 technical support to the petrographic investigations.

561

562

### 563 **3.7 References**

564 Abraitis, P.K., Patrick, R.A.D., Vaughan, D.J., 2004. Variations in the compositional, textural and  
565 electrical properties of natural pyrite: a review. *Int. J. Miner. Process.* 74, 41–59.  
566 <https://doi.org/10.1016/j.minpro.2003.09.002>

567 Audouin, O., Bodin, J., Porel, G., Bourbiaux, B., 2008. Flowpath structure in a limestone aquifer: multi-  
568 borehole logging investigations at the hydrogeological experimental site of Poitiers, France.  
569 *Hydrogeol. J.* 16, 939–950. <https://doi.org/10.1007/s10040-008-0275-4>

570 Bassil, J., Naveau, A., Bueno, M., Di Tullo, P., Grasset, L., Kazpard, V., Razack, M., 2016a.  
571 Determination of the distribution and speciation of selenium in an argillaceous sample using  
572 chemical extractions and post-extractions analyses: application to the hydrogeological experimental  
573 site of Poitiers. *Environ. Sci. Pollut. Res.* 23, 9598–9613. [https://doi.org/10.1007/s11356-016-6113-](https://doi.org/10.1007/s11356-016-6113-7)  
574 [7](https://doi.org/10.1007/s11356-016-6113-7)

575 Bassil, J., Naveau, A., Fontaine, C., Grasset, L., Bodin, J., Porel, G., Razack, M., Kazpard, V., Popescu,  
576 S.-M., 2016b. Investigation of the nature and origin of the geological matrices rich in selenium  
577 within the Hydrogeological Experimental Site of Poitiers, France. *Comptes Rendus Geosci.* 348,  
578 598–608. <https://doi.org/10.1016/j.crte.2016.08.004>

579 Bassil, J., Naveau, A., Bueno, M., Razack, M., Kazpard, V., 2018. Leaching behavior of selenium from  
580 the karst infillings of the Hydrogeological Experimental Site of Poitiers. *Chem. Geol.* 483, 141–150.  
581 <https://doi.org/10.1016/j.chemgeo.2018.02.032>

582 Börsig, N., Scheinost, A.C., Shaw, S., Schild, D., Neumann, T., 2017. Uptake mechanisms of selenium  
583 oxyanions during the ferrihydrite-hematite recrystallization. *Geochim. Cosmochim. Acta* 206, 236–  
584 253. <https://doi.org/10.1016/j.gca.2017.03.004>

585 Chen, C.J., Chen, C.W., Wu, M.M., Kuo, T.L., 1992. Cancer potential in liver, lung, bladder and kidney  
586 due to ingested inorganic arsenic in drinking water. *Br. J. Cancer* 66, 5, 888-892.

587 Chung, F.H., 1975. Quantitative Interpretation of X-Ray Diffraction Patterns. III. Simultaneous  
588 Determination of a Set of Reference Intensities. *J. Appl. Crystallogr.* 8, 17

589 Costagliola, P., Bardelli, F., Benvenuti, M., Di Benedetto, F., Lattanzi, P., Romanelli, M., Paolieri, M.,  
590 Rimondi, V., Vaggelli, G., 2013. Arsenic-Bearing Calcite in Natural Travertines: Evidence from  
591 Sequential Extraction,  $\mu$ XAS, and  $\mu$ XRF. *Environ. Sci. Technol.* 47, 6231–6238.  
592 <https://doi.org/10.1021/es304953a>

593 European Union (1998) Council directive 98/83/EC on the quality of water intended for human  
594 consumption. *Official Journal of the European Communities*, L 330/32, 32–54.

595 Fernández-Martínez, A., Charlet, L., 2009. Selenium environmental cycling and bioavailability: a  
596 structural chemist point of view. *Rev. Environ. Sci. Biotechnol.* 8, 81–110.  
597 <https://doi.org/10.1007/s11157-009-9145-3>

598 Geoffroy, N., Demopoulos, G.P., 2009. Reductive Precipitation of Elemental Selenium from Selenious  
599 Acidic Solutions Using Sodium Dithionite. *Ind. Eng. Chem. Res.* 48, 10240–10246.  
600 <https://doi.org/10.1021/ie9008502>

601 Gustafsson, J.P., Johnsson, L., 1994. The association between selenium and humic substances in  
602 forested ecosystems—laboratory evidence. *Appl. Organomet. Chem.* 8, 141–147.  
603 <https://doi.org/10.1002/aoc.590080209>

604 Hillier S. (2000) – Accurate quantitative analysis of clay and other minerals in sandstones by XRD:  
605 comparison of a Rietveld and a reference intensity ratio (RIR) method and the importance of sample  
606 preparation. *Clay Mineralogy*, 35, 291-302.

607

608 Jansen, B., Tonneijck, F.H., Verstraten, J.M., 2011. Selective Extraction Methods for Aluminium, Iron  
609 and Organic Carbon from Montane Volcanic Ash Soils. *Pedosphere* 21, 549–565.  
610 [https://doi.org/10.1016/S1002-0160\(11\)60157-4](https://doi.org/10.1016/S1002-0160(11)60157-4)

611 Javed, M.B., Kachanoski, G., Siddique, T., 2013. A modified sequential extraction method for arsenic  
612 fractionation in sediments. *Anal. Chim. Acta* 787, 102–110.  
613 <https://doi.org/10.1016/j.aca.2013.05.050>

614 Javed, M.B., Kachanoski, G., Siddique, T., 2014. Arsenic fractionation and mineralogical  
615 characterization of sediments in the Cold Lake area of Alberta, Canada. *Sci. Total Environ.* 500–  
616 501, 181–190. <https://doi.org/10.1016/j.scitotenv.2014.08.083>

617 Jegadeesan, G., Al-Abed, S.R., Pinto, P., 2008. Influence of trace metal distribution on its leachability  
618 from coal fly ash. *Fuel* 87, 1887–1893. <https://doi.org/10.1016/j.fuel.2007.12.007>

619 Kim, E.J., Jeon, E.-K., Baek, K., 2016. Role of reducing agent in extraction of arsenic and heavy metals  
620 from soils by use of EDTA. *Chemosphere* 152, 274–283.  
621 <https://doi.org/10.1016/j.chemosphere.2016.03.005>

622 Kim, E.J., Lee, J.-C., Baek, K., 2015. Abiotic reductive extraction of arsenic from contaminated soils  
623 enhanced by complexation: Arsenic extraction by reducing agents and combination of reducing and  
624 chelating agents. *J. Hazard. Mater.* 283, 454–461. <https://doi.org/10.1016/j.jhazmat.2014.09.055>

625 Kim, E.J., Yoo, J.-C., Baek, K., 2014. Arsenic speciation and bioaccessibility in arsenic-contaminated  
626 soils: Sequential extraction and mineralogical investigation. *Environ. Pollut.* 186, 29–35.  
627 <https://doi.org/10.1016/j.envpol.2013.11.032>

628 Kulp, T.R., Pratt, L.M., 2004. Speciation and weathering of selenium in upper cretaceous chalk and  
629 shale from South Dakota and Wyoming, USA. *Geochim. Cosmochim. Acta* 68, 3687–3701.  
630 <https://doi.org/10.1016/j.gca.2004.03.008>

631 Le Coz, M., Bodin, J., Renard, P., 2017. On the use of multiple-point statistics to improve groundwater  
632 flow modeling in karst aquifers: A case study from the Hydrogeological Experimental Site of  
633 Poitiers, France. *J. Hydrol.* 545, 109–119. <https://doi.org/10.1016/j.jhydrol.2016.12.010>

634 Li, Z., Liang, D., Peng, Q., Cui, Z., Huang, J., Lin, Z., 2017. Interaction between selenium and soil  
635 organic matter and its impact on soil selenium bioavailability: A review. *Geoderma* 295, 69–79.  
636 <https://doi.org/10.1016/j.geoderma.2017.02.019>

637 Mari, J.L., Porel, G., Delay, F. 2020. Contribution of full wave acoustic logging to the detection and  
638 prediction of karstic bodies. *Water*, 12, 948; doi:10.3390/w12040948

639 Martens, D.A., Suarez, D.L., 1997. Selenium Speciation of Soil/Sediment Determined with Sequential  
640 Extractions and Hydride Generation Atomic Absorption Spectrophotometry. *Environ. Sci. Technol.*  
641 31, 133–139. <https://doi.org/10.1021/es960214+>

642 Matamoros-Veloza, A., Newton, R.J., Benning, L.G., 2011. What controls selenium release during  
643 shale weathering? *Appl. Geochem.* 26, S222–S226.  
644 <https://doi.org/10.1016/j.apgeochem.2011.03.109>

645 Nakamaru, Y.M., Altansud J., 2014. Speciation and bioavailability of selenium and antimony in non-  
646 flooded and wetland soils: a review. *Chemosphere* 111, 366–371.

647 Pnias, D., Taxiarchou, M., Paspaliaris, I., Kontopoulos, A., 1996. Mechanisms of dissolution of iron  
648 oxides in aqueous oxalic acid solutions. *Hydrometallurgy* 42, 257–265.  
649 [https://doi.org/10.1016/0304-386X\(95\)00104-O](https://doi.org/10.1016/0304-386X(95)00104-O)

650 Raessler, M., 2018. The Arsenic Contamination of Drinking and Groundwaters in Bangladesh:  
651 Featuring Biogeochemical Aspects and Implications on Public Health. *Arch. Environ. Contam.*  
652 *Toxicol.* 75, 1–7. <https://doi.org/10.1007/s00244-018-0511-4>

653 Renard, F., Putnis, C.V., Montes-Hernandez, G., Ruiz-Agudo, E., Hovelmann, J., Sarret, G., 2015.  
654 Interactions of arsenic with calcite surfaces revealed by in situ nanoscale imaging. *Geochim.*  
655 *Cosmochim. Acta* 159, 61–79. <https://doi.org/10.1016/j.gca.2015.03.025>

656 Rios-Valenciana, E.E., Briones-Gallardo, R., Chazaro-Ruiz, L.F., Lopez-Lozano, N.E., Sierra-Alvarez,  
657 R., Celis, L.B., 2020. Dissolution and final fate of arsenic associated with gypsum, calcite, and  
658 ferrihydrite: Influence of microbial reduction of As(V), sulfate, and Fe(III). *Chemosphere* 239,  
659 124823. <https://doi.org/10.1016/j.chemosphere.2019.124823>

660 Ritsema, C.J., Groenenberg, J.E., Bisdom, E.B.A., 1992. The transformation of potential into actual  
661 acid sulphate soils studied in column experiments. *Geoderma* 55, 259–271.  
662 [https://doi.org/10.1016/0016-7061\(92\)90087-N](https://doi.org/10.1016/0016-7061(92)90087-N)

663 Rosen, B.P., Liu, Z., 2009. Transport pathways for arsenic and selenium: A minireview. *Environ. Int.*  
664 35, 512–515. <https://doi.org/10.1016/j.envint.2008.07.023>

665 Sawlowicz, Z., Łatkiewicz, A., Stefaniak, E., 2005. Two-dimensional natural pyrite crystals and their  
666 formation. *Mineral. Mag.* 69, 455–461. <https://doi.org/10.1180/0026461056940263>

667 Smedley, P.L., Kinniburgh, D.G., 2002. A review of the source, behaviour and distribution of arsenic in  
668 natural waters. *Appl. Geochem.* 17, 517–568. [https://doi.org/10.1016/S0883-2927\(02\)00018-5](https://doi.org/10.1016/S0883-2927(02)00018-5)

669 Smith, A.H., Hopenhayn-Rich, C., Bates, M.N., Goeden, H.M., Hertz-Picciotto, I., Duggan, H.M.,  
670 Wood, R., Kosnett, M.J., Smith, M.T., 1992. Cancer risks from arsenic in drinking water. *Environ.*  
671 *Health Perspect.* 97, 259–267

672 Su, T., Wang, J., 2011. Modeling batch leaching behavior of arsenic and selenium from bituminous coal  
673 fly ashes. *Chemosphere* 85, 1368–1374. <https://doi.org/10.1016/j.chemosphere.2011.08.002>

674 Tabelin, C.B., Igarashi, T., Yoneda, T., 2012. Mobilization and speciation of arsenic from  
675 hydrothermally altered rock containing calcite and pyrite under anoxic conditions. *Appl. Geochem.*  
676 27, 2300–2314. <https://doi.org/10.1016/j.apgeochem.2012.07.020>

677 Tabelin, C.B., Hashimoto, A., Igarashi, T., Yoneda, T., 2014. Leaching of boron, arsenic and selenium  
678 from sedimentary rocks: II. pH dependence, speciation and mechanisms of release. *Sci. Total*  
679 *Environ.* 473–474, 244–253. <https://doi.org/10.1016/j.scitotenv.2013.12.029>

680 Tabelin, C.B., Sasaki, R., Igarashi, T., Park, I., Tamoto, S., Arima, T., Ito, M., Hiroyoshi, N., 2017.  
681 Simultaneous leaching of arsenite, arsenate, selenite and selenate, and their migration in tunnel-  
682 excavated sedimentary rocks: I. Column experiments under intermittent and unsaturated flow.  
683 *Chemosphere* 186, 558–569. <https://doi.org/10.1016/j.chemosphere.2017.07.145>

684 Tamoto, S., Tabelin, C.B., Igarashi, T., Ito, M., Hiroyoshi, N., 2015. Short and long term release  
685 mechanisms of arsenic, selenium and boron from a tunnel-excavated sedimentary rock under in situ  
686 conditions. *J. Contam. Hydrol.* 175–176, 60–71. <https://doi.org/10.1016/j.jconhyd.2015.01.003>

687 Tessier, A., Campbell, P.G.C., Bisson, M., 1979. Sequential extraction procedure for the speciation of  
688 particulate trace metals. *Anal. Chem.* 51, 844–851. <https://doi.org/10.1021/ac50043a017>

689 Wagai, R., Mayer, L.M., Kitayama, K., Shirato, Y., 2013. Association of organic matter with iron and  
690 aluminum across a range of soils determined via selective dissolution techniques coupled with  
691 dissolved nitrogen analysis. *Biogeochemistry* 112, 95–109. <https://doi.org/10.1007/s10533-011-9652-5>

692

693 Wang, Z., Shen, X., Jing, M., Li, C., 2018. Enhanced arsenic removal from drinking water by  
694 FeOOH/ $\gamma$ -Al<sub>2</sub>O<sub>3</sub> granules. *J. Alloys Compd.* 735, 1620–1628.  
695 <https://doi.org/10.1016/j.jallcom.2017.11.284>

696 Wenzel, W.W., Kirchbaumer, N., Prohaska, T., Stingeder, G., Lombi, E., Adriano, D.C., 2001. Arsenic  
697 fractionation in soils using an improved sequential extraction procedure. *Anal. Chim. Acta* 436,  
698 309–323. [https://doi.org/10.1016/S0003-2670\(01\)00924-2](https://doi.org/10.1016/S0003-2670(01)00924-2)

699 Wilkin, R.T., Barnes, H.L., Brantley, S.L., 1996. The size distribution of framboidal pyrite in modern  
700 sediments: An indicator of redox conditions. *Geochim. Cosmochim. Acta* 60, 3897–3912.  
701 [https://doi.org/10.1016/0016-7037\(96\)00209-8](https://doi.org/10.1016/0016-7037(96)00209-8)

702 Wilkin, R.T., Lee, T.R., Beak, D.G., Anderson, R., Burns, B., 2018. Groundwater co-contaminant  
703 behavior of arsenic and selenium at a lead and zinc smelting facility. *Appl. Geochem.* 89, 255–264.  
704 <https://doi.org/10.1016/j.apgeochem.2017.12.011>

705 Xiang Z., Dong L., Hongling B., Liangliang D., Hongmei L., Peng Y., Peixin D., Hongzhe S. (2018)  
706 - XRD-based quantitative analysis of clay minerals using reference intensity ratios, mineral intensity  
707 factors, Rietveld, and full pattern summation methods: A critical review. *Solid Earth Sciences*, 3, 16-29.

708

709 Xu, J., Ding, W., Wu, F., Mailhot, G., Zhou, D., Hanna, K., 2016. Rapid catalytic oxidation of arsenite  
710 to arsenate in an iron(III)/sulfite system under visible light. *Appl. Catal. B Environ.* 186, 56–61.  
711 <https://doi.org/10.1016/j.apcatb.2015.12.033>

712 Yang, H., He, M., 2016. Distribution and Speciation of Selenium, Antimony, and Arsenic in Soils and  
713 Sediments Around the Area of Xikuangshan (China): *Soil. CLEAN - Soil Air Water* 44, 1538–1546.  
714 <https://doi.org/10.1002/clen.201400522>

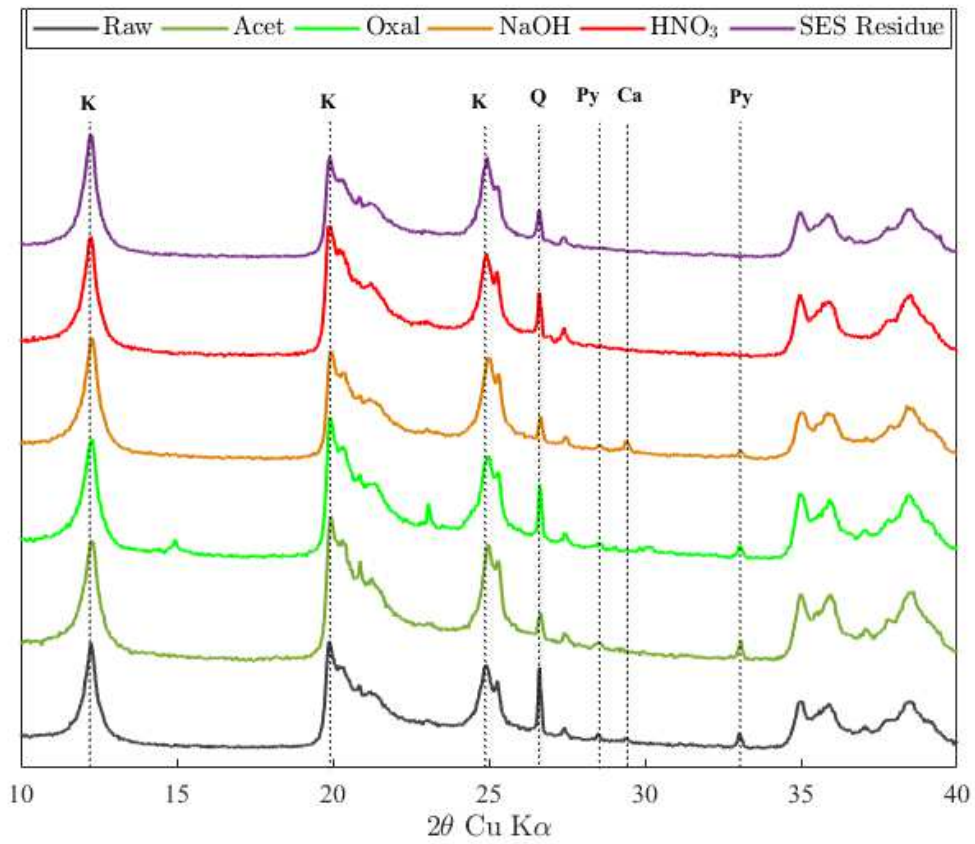
715 Zakharova, E.A., Noskova, G.N., Moskaleva, M.L., Elesova, E.E., Wildgoose, G.G., 2015.  
716 Investigations into the Speciation of Inorganic Arsenic in Weakly Alkaline Medium by  
717 Voltammetry. *Electroanalysis* 27, 890–901. <https://doi.org/10.1002/elan.201500034>

718 Zhang, Y., Jr, W.T.F., 2003. Determination of Selenium Fractionation and Speciation in Wetland  
719 Sediments by Parallel extraction. *Int. J. Environ. Anal. Chem.* 83, 315–326.  
720 <https://doi.org/10.1080/0306731031000076850>

721  
722  
723  
724  
725

726

727 **Figures**



728

729

730 **Figure 1:** X-ray diffraction patterns of the sedimentary sample C5-BjF and the residues after parallel extractions.

731 The patterns were normalized to the intensity of the peak of kaolinite (K) that is not affected by the chemical

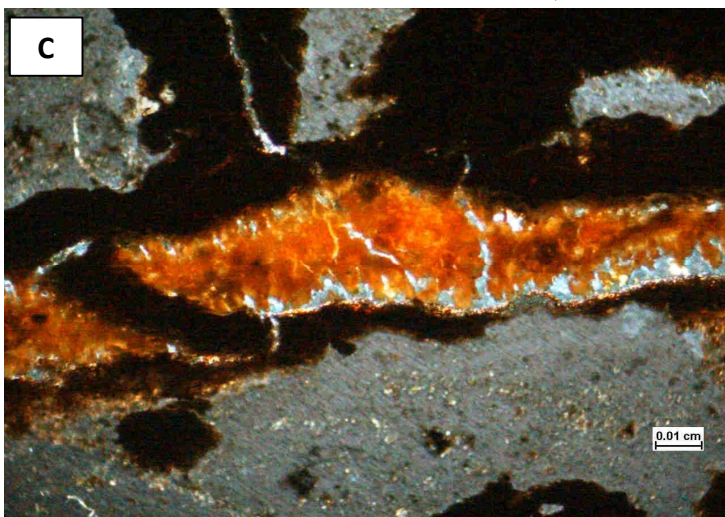
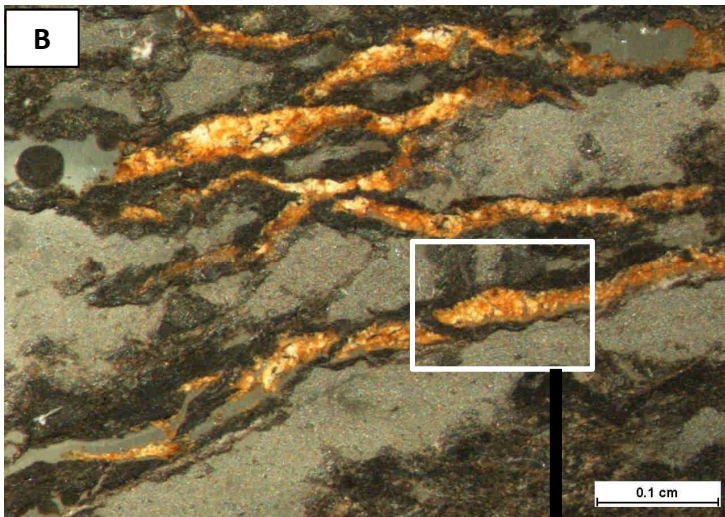
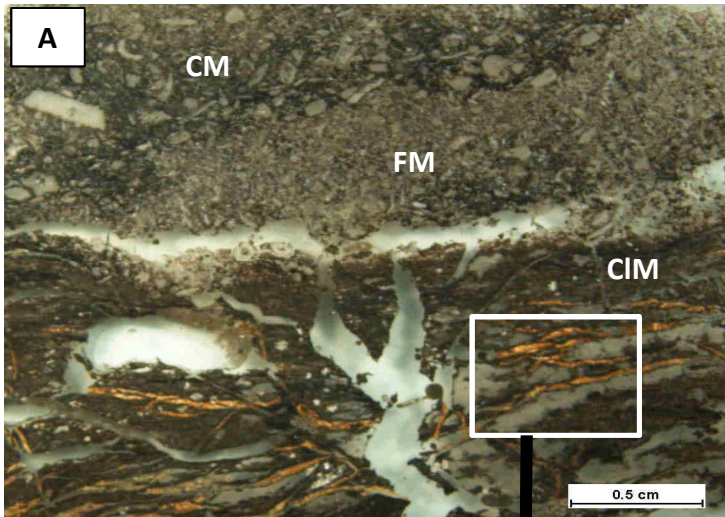
732 extractions. Note the changes in the peak intensities of pyrite (Py) and calcite (Ca) with the different treatments.

733 Q: Quartz.

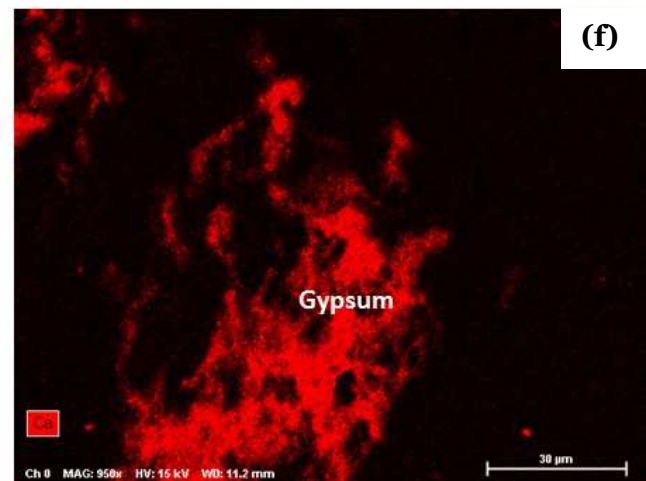
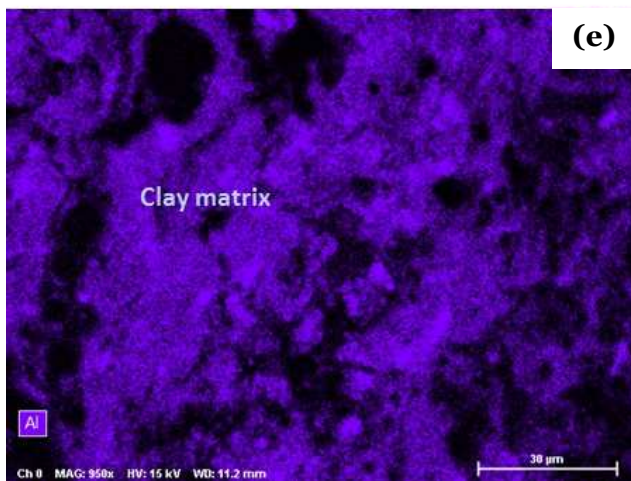
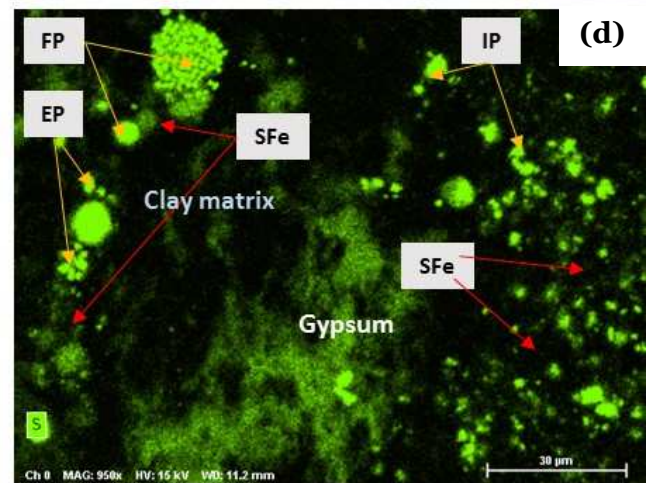
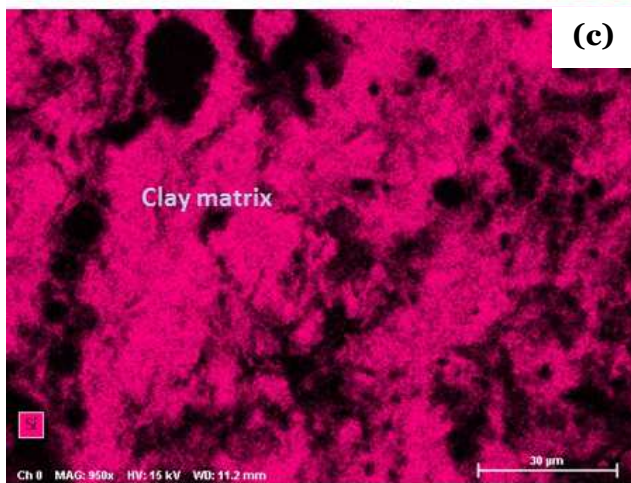
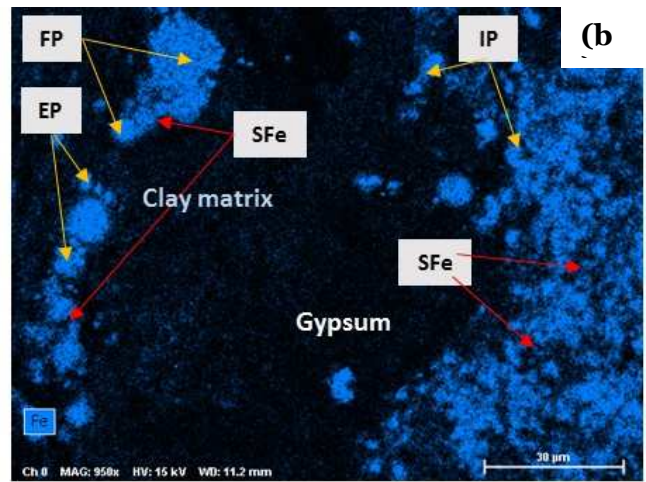
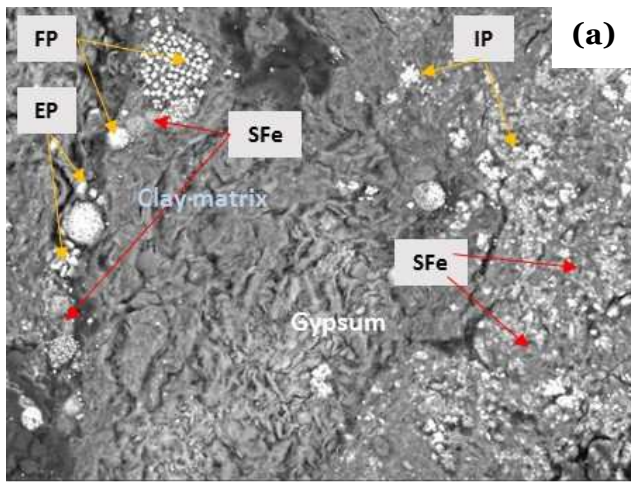
734

735

736

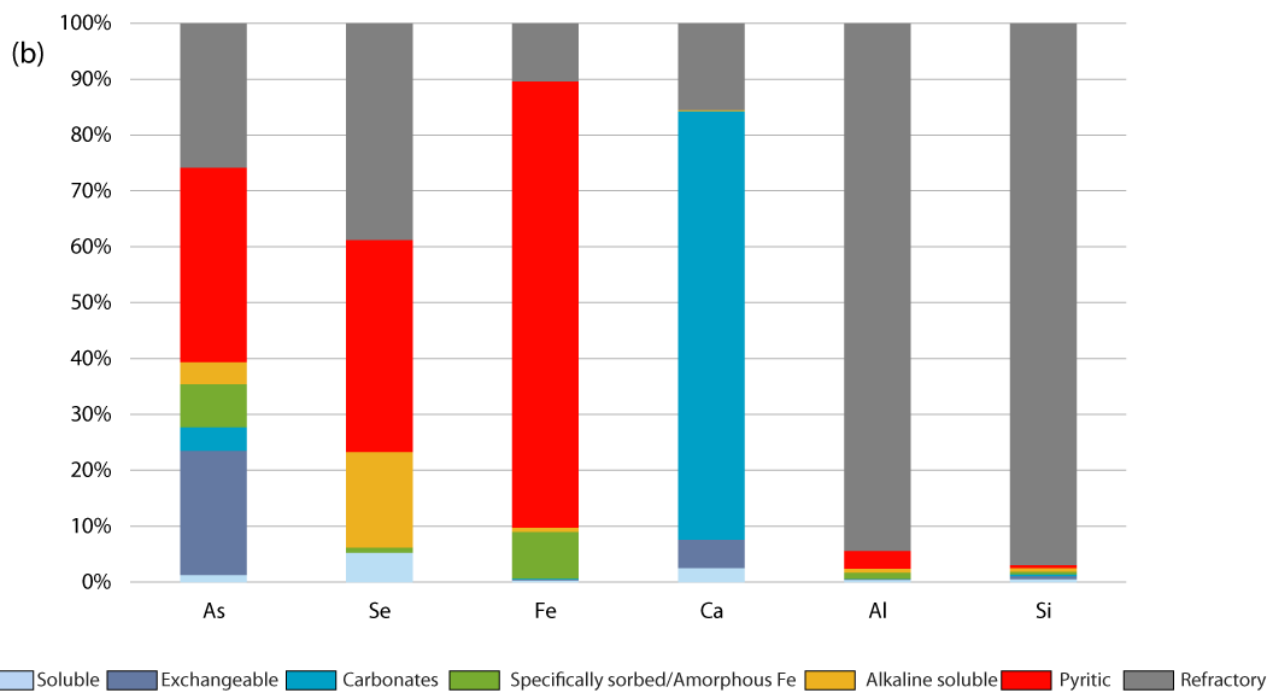
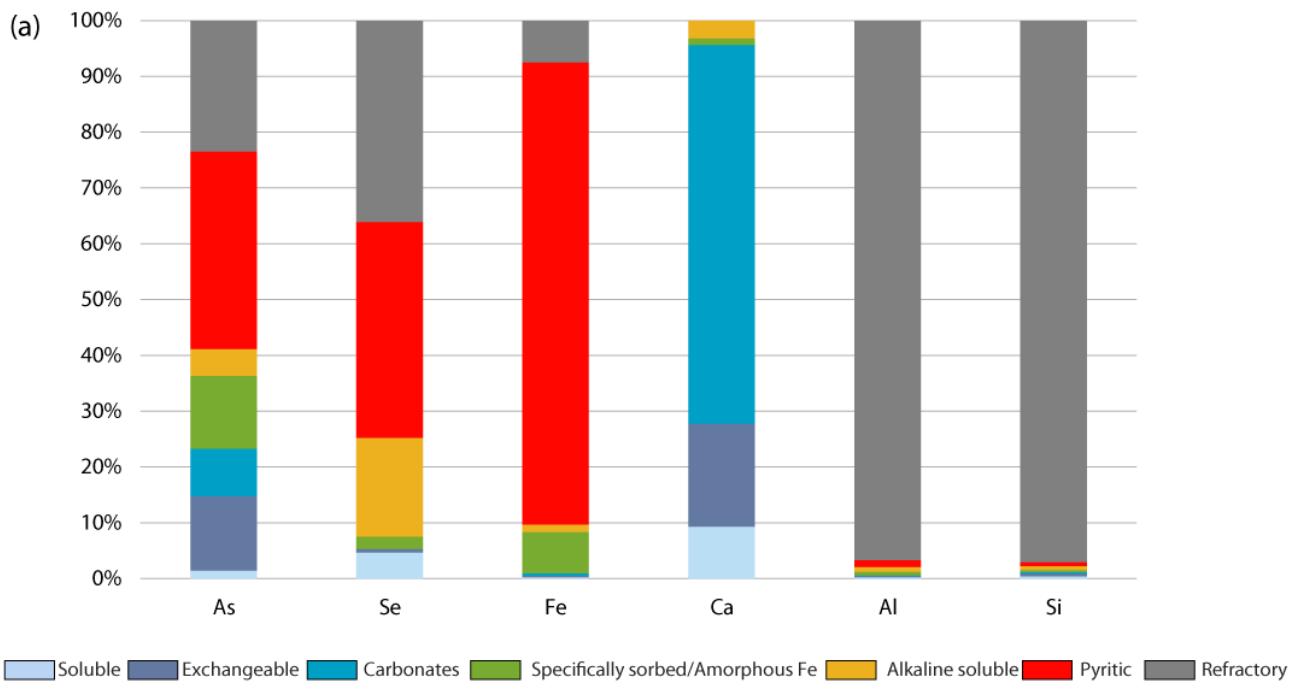


737 **Figure 2:** Petrographic observations on polished thin sections (A) of the sedimentary sample C5-BjF; (B) and (C)  
 738 are detailed view of regions of interest. The infilling material is composed of mixture of carbonates (white) and  
 739 iron oxyhydroxides (ochreous). CM: coarse material, FM: fine material, CIM: clay matrix.



740  
741  
742  
743  
744  
745

**Figure 3:** Scanning electron micrograph (a) of selected area of pyritized clay matrix of the C5-BjF sample, elemental maps for (b) Fe, (c) Si, (d) S, (e) Al, and (f) Ca. Pyrites are identified by the presence of Fe and S; Clay minerals are identified by the presence of Si and Al. Gypsum is identified by presence of Ca and S. FP: framboidal pyrites; EP: euhedral pyrites; IP: intermediate morphology pyrite.



746  
747  
748  
749

**Figure 4:** Released amounts (in percentage) of arsenic, selenium, iron, calcium, aluminum, and silicon for a contact time of 2h (a) and 24h (b) by the sequential extraction scheme.

750  
751  
752  
753  
754  
755  
756  
757  
758  
759  
760  
761  
762  
763  
764  
765  
766  
767  
768  
769  
770  
771  
772

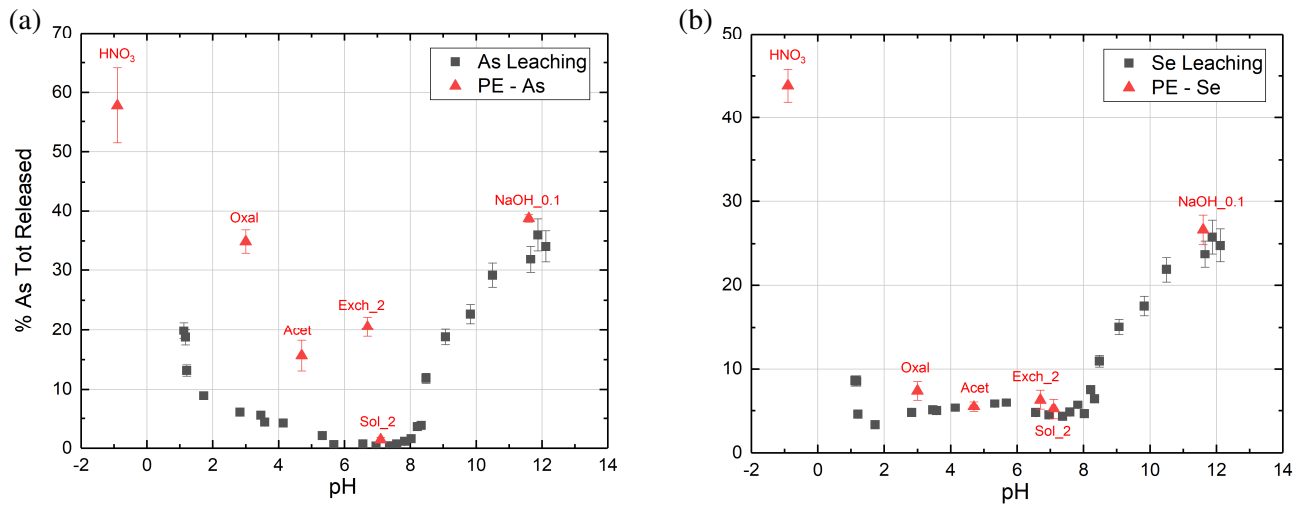
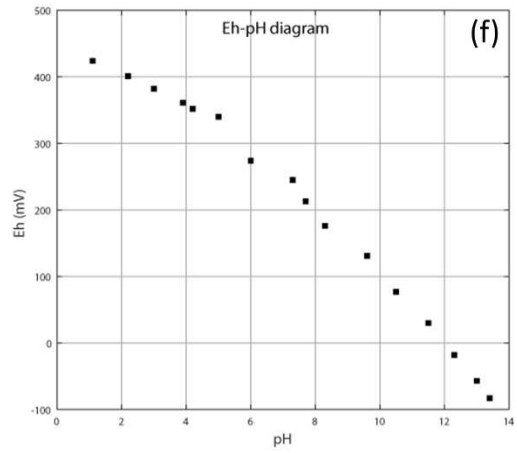
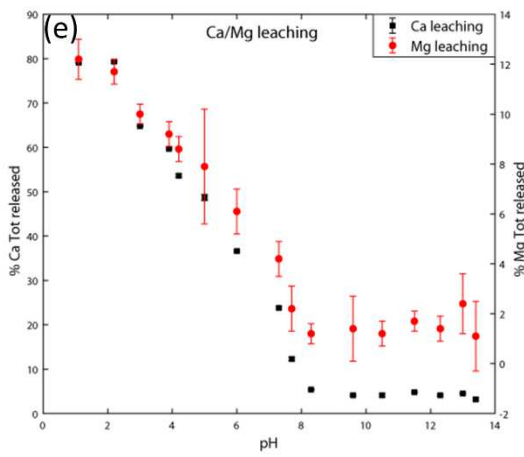
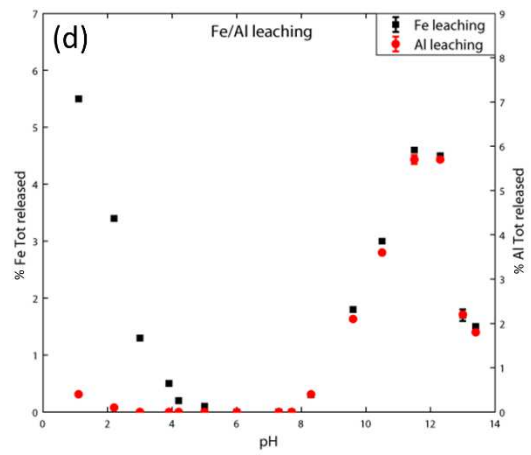
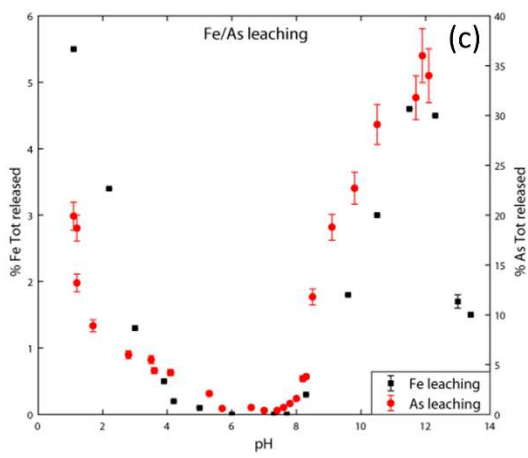
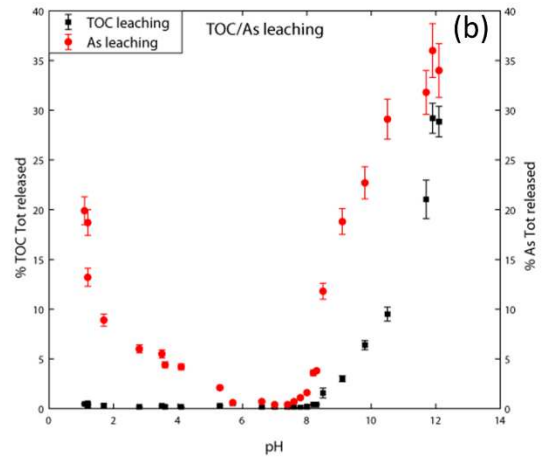
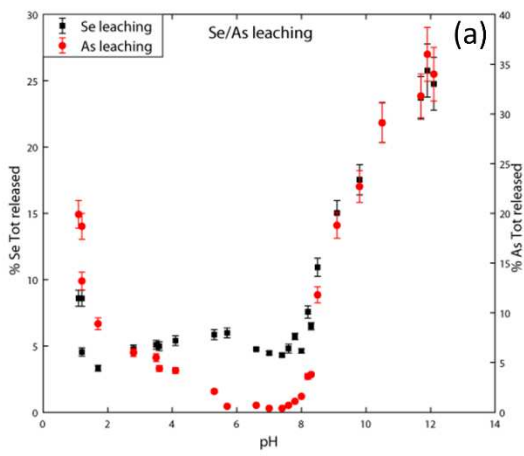


**Figure 5:** Released amounts (in percentage) of (a) arsenic and (b) selenium as a function of pH (contact time of 1 week). PE: Parallel extraction results.



773  
774  
775  
776

**Figure 6:** Released amounts (in percentage) of (a) arsenic/selenium; (b) total organic carbon/arsenic; (c) iron/arsenic; (d) iron/aluminum; (e) calcium/magnesium; (f) Eh as a function of pH (contact time of 1 week)

777  
778  
779  
780  
781

## Tables

**Table 1:** Experimental conditions of the single parallel extractions.

Code	Reagent	Concentration	Exp conditions	pH*	Target/Rule	Comments
Sol_1	H <sub>2</sub> O		30 min, room T	6.8	Soluble fraction	
Sol_2	H <sub>2</sub> O		2h, room T	7.1	Soluble fraction	
Exch_1	NH <sub>4</sub> Sulfate	0.05 M	4h, room T	6.8	Exchangeable fraction	Outer-sphere complexes
Exch_2	NH <sub>4</sub> Phosphate Buffer	0.05 M	2h, room T	6.7	Exchangeable fraction	Inner-sphere complexes
Acet	Na Acetic Buffer	1 M	5h, room T	4.7	Carbonates fraction	Dissolution of carbonates
Oxal	NH <sub>4</sub> Oxalate Buffer	0.2 M	2h, room T, dark	3.0	Specifically sorbed fraction	Strongly adsorbed onto amorphous Fe, Al, and Mn oxides
Red_A	Na Dithionite	0.1 M	24h, room T	5.3	Reducing As fraction (strong)	Co-precipitated with Fe-oxides (strong interactions)
Red_B	Ascorbic Acid	0.1 M	24h, room T	2.6	Reducing As fraction (mild)	Co-precipitated with Fe-oxides (weak interactions)
Red_C	NH <sub>4</sub> Oxalate	0.1 M	24h, room T	6.8	Reducing As fraction (mild)	Co-precipitated with Fe-oxides (weak interactions)
EDTA	EDTA	0.1 M	24h, room T	4.3	Fe Chelatant	To limit the reprecipitation of As
EDTA/Red_A	EDTA/Dithio	0.1 M	24h, room T	4.8	Reducing As fraction	Co-precipitated with Fe-oxides
EDTA/Red_B	EDTA/Asc	0.1 M	24h, room T	3.5	Reducing As fraction	Co-precipitated with Fe-oxides
EDTA/Red_C	EDTA/Ox	0.1 M	24h, room T	5.2	Reducing As fraction	Co-precipitated with Fe-oxides
NaOCl	NaOCl	5%	24h, room T	9.1	Oxidisable Se fraction	Organic Se fraction
Sulf	Na <sub>2</sub> SO <sub>3</sub>	1 M	8h, ultrasonic bath	8.6	Oxidisable Se fraction	Elementary Se fraction
NaOH_1	NaOH	1 M	24h, room T	13.5	Alkaline-soluble fraction	OM associated (humic-like) + Clay fraction
NaOH_0.5	NaOH	0.5 M	24h, room T	13.4	Alkaline-soluble fraction	OM associated (humic-like) + Clay fraction
NaOH_0.1	NaOH	0.1 M	24h, room T	11.6	Alkaline-soluble fraction	OM associated (humic-like) + Clay fraction
HNO <sub>3</sub>	HNO <sub>3</sub>	25%	2h, 70°C	-0.9	Pyritic fraction	Co-precipitated with pyritic materials

\* pH measured in the supernatant after contact time

782  
783  
784  
785

786 **Table 2:** Description of the sequential extraction scheme.

787

<b>Code</b>	<b>Reagent</b>	<b>Concentration</b>	<b>Exp. conditions</b>	<b>pH</b>	<b>Target</b>
Sol_2	H <sub>2</sub> O		2h/24h, room T	7.1	Soluble fraction
Exch_2	NH <sub>4</sub> Phosphate Buffer	0.05 M	2h/24h, room T	6.7	Exchangeable fraction
Acet	Na Acetic Buffer	1 M	5h/24h, room T	4.7	Carbonates
Oxal	NH <sub>4</sub> Oxalate Buffer	0.2 M	2h/24h, room T, dark	3.0	Amorphous Fe fraction
NaOH_0.1	NaOH	0.1 M	24h, room T	11.6	Alkaline-soluble fraction
HNO <sub>3</sub>	HNO <sub>3</sub>	25%	2h/24h, 70 °C	-0.9	Pyritic fraction

788 \*: pH measured in the supernatant after the contact time

789

790

791

792

793

794 **Table 3:** Chemical and mineralogical composition of the C5-BjF (this study) and C5-BjC samples (Bassil et al. 2018).  
 795

Sample	SiO <sub>2</sub> %	Al <sub>2</sub> O <sub>3</sub> %	Fe <sub>2</sub> O <sub>3</sub> %	FeO %	MnO %	MgO %	CaO %	Na <sub>2</sub> O %	K <sub>2</sub> O %	TiO <sub>2</sub> %	org. C %	S Total %
C5-BjF	40.6	30.4	1.8	1.1	< DL	0.3	1.1	0.04	0.07	1.82	5.7	0.57
C5-BjC <sup>a</sup>	39.5	29.2	1.7	ND	< DL	0.3	1.2	0.03	0.06	1.74	8.8	0.61

Sample	As mg/kg	Se mg/kg	Pb mg/kg	Th mg/kg	U mg/kg	Σ REE mg/kg	Ce mg/kg	La mg/kg	Ba mg/kg	Cs mg/kg	Rb mg/kg	Sr mg/kg
C5-BjF	22.4	6.3	56.6	24.3	14.4	812.8	315.5	177.6	19.9	1.4	4.6	20.9
C5-BjC <sup>a</sup>	20.8	2.5	58.9	23.0	47.3	313.4	313.4	178.7	22.2	1.3	4.2	22.4

Sample	Depth m	Calcite %	Pyrite %	Quartz %	Microcline %	Anatase %	Rutile %	Total clay minerals %	SSA m <sup>2</sup> g <sup>-1</sup>
C5-BjF	67.9	5.0	1.5	10.0	8.0	5.5	-	71	52.2
C5-BjC <sup>a</sup>	68.0	3.0	3.5	3.0	-	8.0	2.0	80	58.6

<sup>a</sup>Bassil et al. 2018

ND: not determined, < DL: inferior detection limit

796  
 797  
 798  
 799  
 800  
 801  
 802

803  
804**Table 4:** Quantifications of the amounts released (in percentage) by single parallel extractions of the sedimentary sample C5-BjF.

<b>Code</b>	<b>% As</b>	<b>SD</b>	<b>% Se</b>	<b>SD</b>	<b>% Fe</b>	<b>SD</b>	<b>% Ca</b>	<b>SD</b>	<b>% Mg</b>	<b>SD</b>	<b>% Al</b>	<b>SD</b>	<b>% Si</b>	<b>SD</b>
Sol_1	<b>1.3</b>	0.0	<b>4.2</b>	0.1	<b>0.3</b>	0.3	<b>2.0</b>	0.1	<b>0.5</b>	0.0	<b>0.2</b>	0.0	<b>0.2</b>	0.0
Sol_2	<b>1.4</b>	0.4	<b>5.2</b>	1.2	<b>0.2</b>	0.2	<b>8.8</b>	1.8	<b>0.6</b>	0.0	<b>0.3</b>	0.0	<b>0.3</b>	0.1
Exch_1	<b>0.5</b>	0.0	<b>3.7</b>	0.3	<b>0.0</b>	0.0	<b>71.5</b>	2.1	<b>11.6</b>	0.5	<b>0.1</b>	0.0	<b>0.1</b>	0.0
Exch_2	<b>20.6</b>	1.7	<b>6.3</b>	1.2	<b>0.1</b>	0.2	<b>8.4</b>	0.7	<b>6.6</b>	0.7	<b>0.1</b>	0.0	<b>0.1</b>	0.0
Acet	<b>15.7</b>	2.6	<b>5.5</b>	0.6	<b>0.2</b>	0.1	<b>98.2</b>	3.1	<b>13.7</b>	3.1	<b>0.3</b>	0.0	<b>0.1</b>	0.0
Oxal	<b>34.9</b>	2.0	<b>7.4</b>	1.1	<b>5.7</b>	1.0	<b>0.0</b>	0.0	<b>13.4</b>	0.8	<b>0.8</b>	0.1	<b>0.2</b>	0.0
Red_A	<b>20.8</b>	0.5	<b>19.6</b>	0.9	<b>0.5</b>	0.0	<b>77.5</b>	7.0	<b>13.4</b>	1.5	<b>0.2</b>	0.0	<b>0.3</b>	0.0
Red_B	<b>29.3</b>	0.4	<b>17.7</b>	1.1	<b>3.1</b>	0.2	<b>48.8</b>	4.4	<b>8.9</b>	1.0	<b>0.7</b>	0.0	<b>0.3</b>	0.0
Red_C	<b>26.8</b>	0.5	<b>7.8</b>	0.4	<b>2.0</b>	0.2	<b>0.0</b>	0.0	<b>13.1</b>	1.5	<b>0.6</b>	0.0	<b>0.3</b>	0.0
EDTA	<b>28.0</b>	0.4	<b>6.6</b>	0.4	<b>6.0</b>	0.5	<b>100.0</b>	27.6	<b>12.4</b>	1.4	<b>0.6</b>	0.0	<b>0.2</b>	0.0
EDTA/Red_A	<b>29.8</b>	0.7	<b>19.1</b>	0.9	<b>6.1</b>	0.5	<b>100.0</b>	27.5	<b>12.3</b>	1.4	<b>0.7</b>	0.0	<b>0.3</b>	0.0
EDTA/Red_B	<b>30.6</b>	0.8	<b>5.0</b>	0.4	<b>5.5</b>	0.4	<b>100.0</b>	29.2	<b>11.2</b>	1.3	<b>0.8</b>	0.0	<b>0.4</b>	0.0
EDTA/Red_C	<b>31.4</b>	0.7	<b>9.8</b>	0.9	<b>6.1</b>	0.5	<b>18.4</b>	1.7	<b>14.3</b>	1.6	<b>0.7</b>	0.0	<b>0.3</b>	0.0
NaOCl	<b>18.2</b>	4.5	<b>37.3</b>	5.5	<b>0.5</b>	0.4	<b>11.7</b>	1.7	<b>6.5</b>	0.7	<b>0.2</b>	0.0	<b>0.2</b>	0.0
Sulf	<b>40.0</b>	8.1	<b>23.1</b>	1.3	<b>1.8</b>	2.5	<b>4.7</b>	0.4	<b>2.6</b>	0.3	<b>0.6</b>	0.0	<b>0.1</b>	0.0
NaOH_1	<b>38.6</b>	0.8	<b>26.0</b>	1.3	<b>1.2</b>	0.4	<b>3.8</b>	1.8	<b>0.0</b>	0.0	<b>1.0</b>	0.1	<b>0.9</b>	0.1
NaOH_0.5	<b>38.9</b>	0.9	<b>26.3</b>	1.2	<b>1.4</b>	0.5	<b>7.3</b>	3.5	<b>0.1</b>	0.1	<b>1.2</b>	0.1	<b>0.6</b>	0.0
NaOH_0.1	<b>38.8</b>	0.6	<b>26.6</b>	1.7	<b>7.2</b>	2.5	<b>7.8</b>	3.7	<b>5.4</b>	3.0	<b>7.7</b>	0.5	<b>0.4</b>	0.0
HNO <sub>3</sub>	<b>57.8</b>	6.3	<b>43.8</b>	1.9	<b>90.5</b>	16.4	<b>83.7</b>	28.2	<b>15.4</b>	5.4	<b>2.0</b>	0.1	<b>0.5</b>	0.0

805